Controllable Nondegenerate p-Type Doping of Tungsten Diselenide by Octadecyltrichlorosilane

Dong-Ho Kang,[†] Jaewoo Shim,[†] Sung Kyu Jang,[‡] Jeaho Jeon,[‡] Min Hwan Jeon,[‡] Geun Young Yeom,[‡] Woo-Shik Jung,[§] Yun Hee Jang,[∥] Sungjoo Lee,[*,†,‡,⊥] and Jin-Hong Park[*,†]

[†]School of Electronics & Electrical Engineering and [‡]SKKU Advanced Institute of Nanotechnology (SAINT), Sungkyunkwan University, Suwon 440-746, Korea, [§]Department of Electrical Engineering, Stanford University, Stanford, California 94305 United States, [∥]School of Materials Science and Engineering, Gwangju Institute of Science and Technology, Gwangju 500-712, Korea, and [⊥]Center for Human Interface Nanotechnology (HINT), Suwon 440-746, Korea

ABSTRACT Despite heightened interest in 2D transition-metal dichalcogenide (TMD) doping methods for future layered semiconductor devices, most doping research is currently limited to molybdenum disulfide (MoS_2), which is generally used for n-channel 2D transistors. In addition, previously reported TMD doping techniques result in only high-level doping concentrations (degenerate) in which TMD materials behave as near-metallic layers. Here, we demonstrate a controllable nondegenerate p-type doping (p-doping) technique on tungsten diselenide (WSe_2) for p-channel 2D transistors by adjusting the concentration of octadecyltrichlorosilane (OTS).

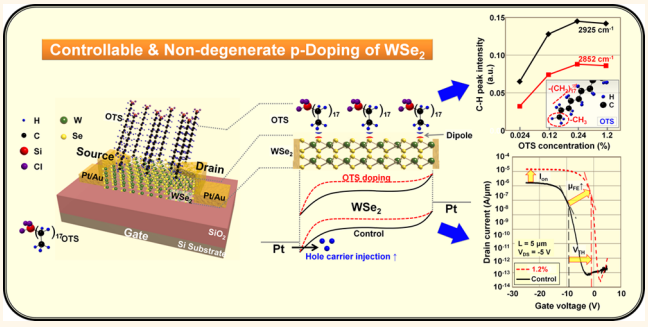

This p-doping phenomenon originates from the methyl ($-CH_3$) functional groups in OTS, which exhibit a positive pole and consequently reduce the electron carrier density in WSe_2. The controlled p-doping levels are between 2.1×10^{11} and 5.2×10^{11} cm^{-2} in the nondegenerate regime, where the performance parameters of WSe_2-based electronic and optoelectronic devices can be properly designed or optimized (threshold voltage↑, on-/off-currents↑, field-effect mobility↑, photoresponsivity↓, and detectivity↓ as the doping level increases). The p-doping effect provided by OTS is sustained in ambient air for a long time showing small changes in the device performance (18−34% loss of ΔV_{TH} initially achieved by OTS doping for 60 h). Furthermore, performance degradation is almost completely recovered by additional thermal annealing at 120 °C. Through Raman spectroscopy and electrical/optical measurements, we have also confirmed that the OTS doping phenomenon is independent of the thickness of the WSe_2 films. We expect that our controllable p-doping method will make it possible to successfully integrate future layered semiconductor devices.

KEYWORDS: OTS · WSe_2 · nondegenrate doping · electronic device · optoelectronic device

Two-dimensional (2D) transition-metal dichalcogenides (TMDs) with layered structures are considered promising materials for next-generation wearable, flexible, stretchable, and transparent electronics because of their superior electrical, optical, and mechanical properties.[1−13] Because their thickness is scalable down to a monolayer and they exhibit a van der Waals epitaxial structure without surface dangling bonds, TMD-based thin film transistors (TFTs) are free of the short channel effect (SCE) and carrier mobility degradation caused by surface oxidation/scattering.[1,2] TMDs are also expected to be popular in optoelectronic applications for wide-spectral photodetectors and light emitting diodes (LEDs) because their energy bandgap varies with layer thickness.[5−12] However, the lack of a reliable and controllable doping method, which is essential for inducing a Fermi level shift that subsequently enables modulations of electrical and optical properties, currently prevents such TMD-based electronic and optoelectronic devices from being successfully integrated.

Although much work is currently being done in the field of doping in TMDs, most of it is limited to molybdenum disulfide (MoS_2),[15−20] which forms a low electron barrier contact with metals and is generally used for n-channel transistors. As a result, more research is needed on the doping of tungsten diselenide (WSe_2), which shows a

* Address correspondence to jhpark9@skku.edu, leesj@skku.edu.

Received for review July 1, 2014 and accepted January 26, 2015.

Published online January 28, 2015
10.1021/nn5074435

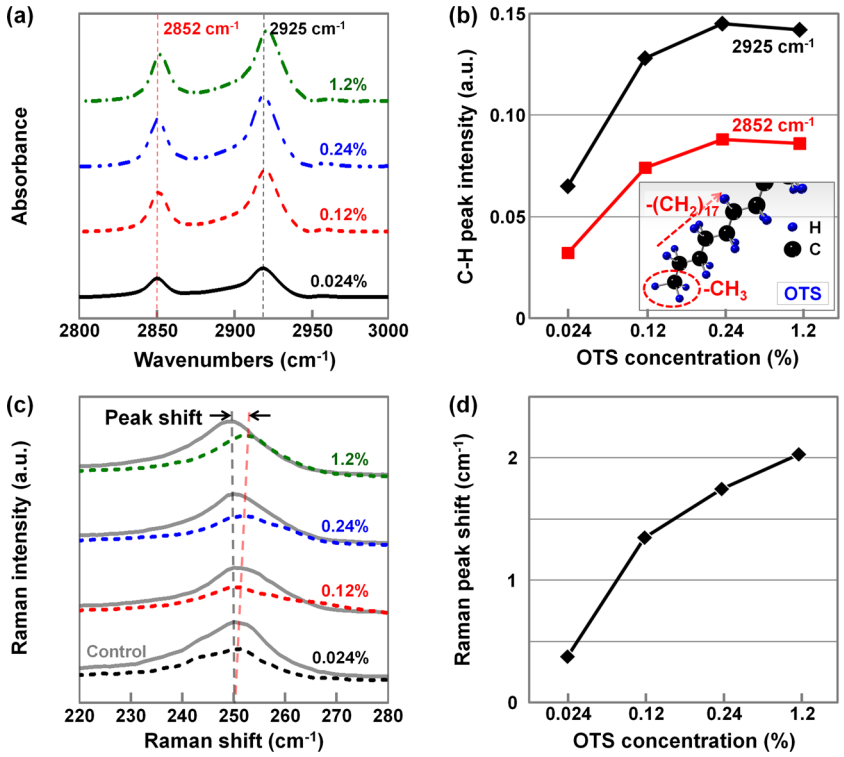

Figure 1. (a) FT-IR spectra of WSe_2 films doped by OTS at different concentrations (0.024%, 0.12%, 0.24%, and 1.2%) and (b) C−H peak intensity data as a function of OTS concentration extracted from the peaks at 2852 and 2925 cm^{-1}. Inset: schematic diagram of OTS with $-CH_3$ and $-(CH_2)_{17}$ groups. (c) Raman spectra of the OTS-doped WSe_2 films and (d) Raman peak shift data as a function of OTS concentration extracted from the peaks at 250 cm^{-1}.

relatively low hole barrier contact with metals and can therefore be used to integrate p-channel transistors to realize 2D TMD-based applications. Fang *et al.* reported an NO_2 molecule-based p-doping[14] and potassium-based n-doping process[15] on WSe_2 using the surface charge-transfer mechanism. They used it to form highly p-/n-doped source/drain (S/D) regions in p-/n-channel TMD-based TFTs. They also controlled the n-doping level by adjusting the exposure time to potassium, but both the p-/n-doping techniques resulted in high-level doping concentrations (degenerate) in which WSe_2 behaved as a near-metallic layer. Therefore, doping controllability in a light doping regime (nondegenerate), in which WSe_2 serves as a semiconducting material, is a critical point in the design and fabrication of WSe_2-based electronic and optoelectronic devices. However, it is difficult to achieve nondegenerate doping on 2D semiconductors (including TMDs) in a controllable fashion because the precisely controllable ion implantation technique cannot be applied to the doping because of crystal damage that occurs while implanting. Here, we demonstrate a controllable nondegenerate p-doping technique on trilayer, few layer, and bulk WSe_2 films by octadecyltrichlorosilane (OTS). Methyl ($-CH_3$) functional groups in OTS have a positive pole and consequently reduce the electron carrier density in WSe_2, showing a p-doping phenomenon. We have systematically investigated the proposed p-doping method in terms of controllability and air-stability through Fourier transform infrared spectroscopy (FT-IR), Raman spectroscopy, capacitance−voltage ($C-V$) measurement, and electrical/optical measurements (I_D-V_G and I_D-V_D with/without exposure to a 785 nm wavelength laser). By adjusting the concentration of OTS in hexane, we control the p-doping level of WSe_2, which can affect the performance (threshold voltage, on-/off-currents, mobility, photoresponsivity, and detectivity) of WSe_2-based electronic and optoelectronic devices. The p-doping effect by OTS is sustained in ambient air for a long time with only small changes in the device performance. Furthermore, performance can also be almost completely recovered by a thermal annealing process.

RESULTS AND DISCUSSION

Formation and Doping Control of OTS on WSe_2 Films. First, we performed FT-IR and Raman spectroscopy analyses on OTS/WSe_2/SiO_2 samples to investigate, respectively, (1) the controllability of OTS concentration in hexanes and (2) the doping effect of OTS on WSe_2. Figure 1 shows (a) the FT-IR spectra (between 2800 and 3000 cm^{-1}) measured on the OTS/WSe_2/SiO_2 samples with different OTS concentrations (0.024%, 0.12%, 0.24%, and 1.2%) and (b) the extracted C−H peak intensity as a function of OTS concentration. We found that the peaks for the $-CH_2$ groups in a long alkyl group chain ($-(CH_2)_{17}$) of OTS are at 2852 and 2925 cm^{-1},[21] and their peak intensity increased as

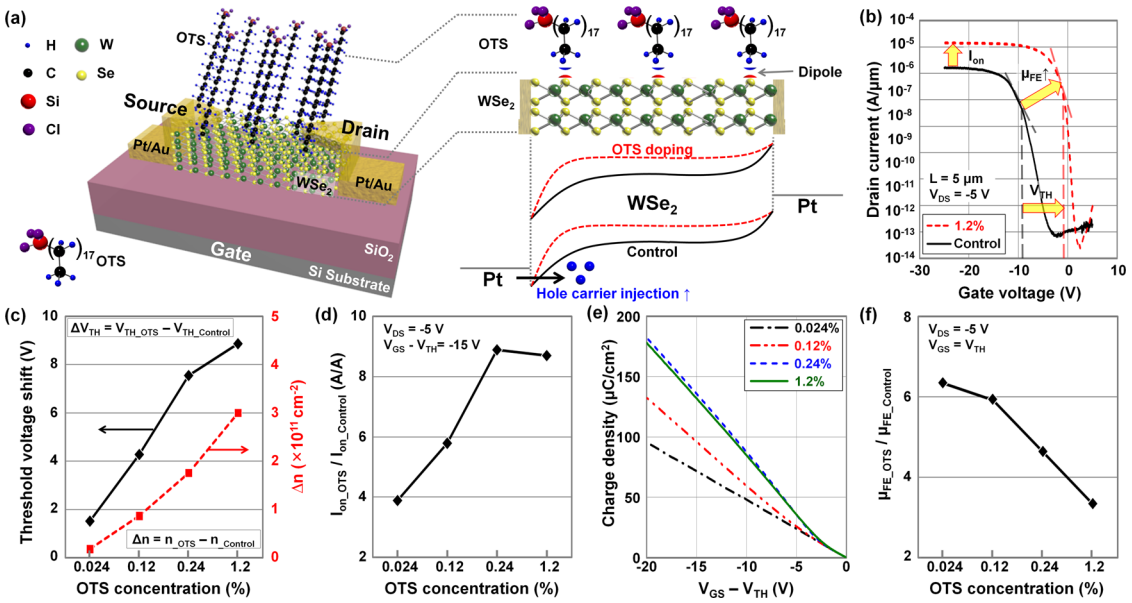

Figure 2. (a) Schematic diagrams of back-gated transistor fabricated on OTS-doped WSe_2 and the energy band diagrams of Pt−WSe_2−Pt junctions. (b) I_D−V_G characteristics of the transistors fabricated on (black) undoped and (red) 1.2% OTS-doped WSe_2 films (L = 5 μm and V_{DS} = −5 V). (c) Threshold voltage shift ($\Delta V_{TH} = V_{TH\text{-}OTS} - V_{TH\text{-}Control}$) and carrier concentration increase ($\Delta n = n_{OTS} - n_{Control}$) as a function of OTS concentration (0.024%, 0.12%, 0.24%, and 1.2%). (d) On-current ratio (I_{on} ratio = $I_{on\text{-}OTS}/I_{on\text{-}Control}$) at $V_{GS} - V_{TH}$ = −15 V and V_{DS} = −5 V as a function of OTS concentration. (e) Charge density *vs* $V_{GS} - V_{TH}$, measured on Pt-OTS-doped WSe_2−SiO_2−Si back gate structure. (f) Field-effect mobility ratio (μ_{FE} ratio = $\mu_{FE\text{-}OTS}/\mu_{FE\text{-}Control}$) at $V_{GS} = V_{TH}$ and V_{DS} = −5 V as a function of OTS concentration.

the OTS concentration rose from 0.024% to 0.24%. Although the OTS concentration was successfully controlled below 0.24%, the peak intensity was saturated above 0.24%, indicating that a high OTS concentration was already achieved in the 0.24% sample. Parts c and d, respectively, of Figure 1 present the Raman spectra measured on the OTS/WSe_2 samples and their peak shift values extracted after performing a 120 °C anneal for the formation of OTS layers. Because both the E^1_{2g} and A^1_g modes for WSe_2 are close to 250 cm^{-1}, we found only a single peak at ~250 cm^{-1}.[7] The blue-shift of the single peak after OTS formation seems to be related to the p-doping phenomenon, based on the Raman peak changes previously reported on doped MoS_2.[19,22] However, Javey *et al.* and Chen *et al.* recently reported inconsistent Raman peak shift results, observing no change after p-doping of WSe_2 by NO_x[23] and a red-shift after Au nanoparticle-based p-doping,[24] respectively. Further research related to Raman analysis of p-doped WSe_2 films will be needed to resolve this issue. As shown in Figure 1d, this blue-shift value continuously increased from 0.372 to 2.028 cm^{-1} as the OTS concentration increased from 0.024% to 1.2%, probably indicating that a higher p-doping level on WSe_2 is achieved by a more highly concentrated OTS layer. Although the Raman peak shift was observed in the WSe_2 samples treated by various solvents used in this work (Δ = 0.08 cm^{-1} for DI water, 0.08 cm^{-1} for acetone, 0.12 cm^{-1} for IPA, 0.17 cm^{-1} for hexane, and 0.01 cm^{-1} for toluene), it was negligibly small compared with that of OTS-doped samples (0.372−2.028 cm^{-1}).

Electrical Characterization of OTS-Doped WSe_2 Electronic Devices. Figure 2a shows a schematic diagram of a WSe_2 transistor doped by an OTS layer along with the energy band diagram of Pt-undoped/doped WSe_2−Pt junctions with a negative V_{DS}. To reconfirm the p-doping phenomenon on WSe_2 shown in the previous Raman spectroscopy analysis, I_D−V_G and C−V characteristics of the doped WSe_2 transistors were investigated with OTS concentrations between 0.024% and 1.2%. The lateral electric field ($E_{Lateral}$) between the source and drain electrodes was fixed at −1 V/μm (V_{DS}/L = −5 V/5 μm). Compared to the control sample (undoped WSe_2), electron carriers further accumulated at the interface between OTS and WSe_2 because the CH_3 group in OTS has positive pole,[20] subsequently making the WSe_2 region p-doped. This p-doping phenomenon on WSe_2 by the formation of a molecular dipole eventually influenced the tunneling of hole carriers from the source to the WSe_2. As shown in Figure 2a, the WSe_2 energy band is shifted up by the p-doping, and it increases the electric field at the source−WSe_2 junction, thereby causing the Schottky barrier lowering effect, enhancing the tunneling of holes and reducing the contact resistance. This effect becomes severe when a higher electric field is applied to a metal−semiconductor junction, according to $\Phi_{H,eff} = \Phi_H - \Delta\Phi_H$, where $\Delta\Phi_H = [(qE)/(4\pi\varepsilon)]^{1/2}$. However, this effect is not expected to occur in the other drain−WSe_2 junction because the bend shift by p-doping decreases the electric field there. As a result, a positive shift in threshold voltage (V_{TH}) from −9.1 V to

−0.45 V (ΔV_{TH} = +8.65 V) was observed after WSe_2 p-doping using a 1.2% OTS layer. In addition, the on-current was increased by about 10 times from 1.64 × 10^{-6} A/μm to 1.42 × 10^{-5} A/μm, also improving the field-effect mobility (μ_{FE}). This mobility improvement is thought to originate from an inaccurate mobility extraction method that does not exclude the effect of contact resistance.[1] We then confirmed the possibility of controlling ΔV_{TH} by adjusting OTS concentration, as shown in Figure 2c. A further positive shift in V_{TH} was observed as the OTS concentration increased from 0.024% to 1.2% because a more concentrated OTS layer with more positive charges attracted more electrons to the OTS−WSe_2 interface, subsequently increasing the p-doping level in WSe_2. The 2D sheet doping concentration (n) extracted from the relation $n = I_D L/qW\mu V_{DS}$ is also consistent with the rising trend in V_{TH} as a function of OTS concentration, showing a significant increase in Δn (= $n_{OTS} - n_{Control}$) from 1.6 × 10^{10} to 3.0 × 10^{11} cm^{-2}. Based on previously reported concentration data (~2.5 × 10^{12} cm^{-2} for potassium-doped WSe_2 and ~2.2 × 10^{12} cm^{-2} for NO_2-doped WSe_2),[14,15] our p-doping concentration level (between 2.1 × 10^{11} and 5.2 × 10^{11} cm^{-2}) seems to be in the nondegenerate regime. In Figure 2d, which shows the on-current ratio (= $I_{onOTS}/I_{onControl}$) as a function of OTS concentration, we also observed that an increase degree in on-current after OTS doping becomes stronger as the OTS concentration increases. Thus, more hole carriers might accumulate at the WSe_2−SiO_2 interface at the same V_{GS} (= V_{TH} − 15 V) bias because of reduced effective hole barrier height for carrier injection (from source to WSe_2) through OTS doping. To support that claim, we measured the C−V characteristics on the OTS-doped WSe_2 samples and plotted the extracted charge density (Q) from the C−V curves as a function of $V_{GS} - V_{TH}$ in Figure 2e. A more detailed explanation of the charge density extraction from C−V characteristics is in Supporting Information (Figure S2). As the V_{GS} negatively increases beyond V_{TH}, the hole charge density increases because hole carriers begin coming to the WSe_2−SiO_2 interface through WSe_2 from the metal contact. In particular, the amount of accumulated hole carriers increases from 71.7 to 132 μC/cm^2 at $V_{GS} - V_{TH}$ = −15 V as the OTS concentration increases to 1.2%. Here, the contact resistance ($R_{Contact}$) in the Pt−WSe_2 junction seems to cause a voltage drop ($V_{Contact}$) that reduces the effective voltage (= $V_{Applied} - V_{Contact}$) applied to the SiO_2 region. When OTS doping concentration increases, we expect the contact resistance to be reduced because of the decrease in the effective hole barrier height. Because of this contact resistance reduction effect in highly OTS-doped devices, at a negative V_{GS} lower than V_{TH}, a higher effective voltage seems to be applied on the SiO_2, consequently increasing its charge density. However, the hole carrier density was saturated beyond 0.24% OTS, which coincides with the saturation phenomenon in the on-current ratio. As shown in Figure 2f and the Supporting Information (Figure S1b), we also extracted field-effect mobility data at V_{DS} = −5 V and $V_{GS} = V_{TH}$ and observed that the initial values (30 ± 4 cm^2 V^{-1} s^{-1}) of the control devices increased up to ~192 cm^2 V^{-1} s^{-1} in the 0.024% OTS-doped sample (~105 cm^2 V^{-1} s^{-1} in the 1.2% OTS-doped sample). Field-effect mobility of 110−250 cm^2/(V s) was previously reported in WSe_2-based TFTs.[2,14,15] The mobility values (105−192 cm^2/(V s) in 0.024−1.2%) extracted at $V_{GS} = V_{TH}$ in this work, which we used for the calculation of carrier concentration, are comparable to the reported values. In particular, the maximum value obtained at different V_{GS} (= V_{TH} − 1 V) is ~250 cm^2/(V s) in the case of a 0.024% OTS-doped device, which is the same as the highest mobility value previously reported. We reconfirmed the p-type doping controllability of WSe_2 by adjusting the OTS concentration based on the observation that the degree of increase in the field-effect hole mobility decreased as a function of OTS concentration. The reduction in field-effect hole mobility can be attributed to the increased scattering probability at the channel region caused by a higher accumulated hole concentration.

Air-Stability Analysis of OTS-Doped Electronic WSe_2 Devices. We then monitored the extracted V_{TH} values on the OTS-doped WSe_2 transistors according to air-exposure time to evaluate the air-stability of the doping. Figure 3a shows the V_{TH} shift values as a function of air-exposure time in WSe_2 transistors with different p-doping levels. The V_{TH} values positively shifted by OTS doping move in the negative direction for the first 60 h of air-exposure time, indicating that the degree of p-doping is relieved during air-exposure. However, we found a small V_{TH} shift phenomenon beyond 60 h of air-exposure compared to what we observed for the first 60 h. In the case of highly doped WSe_2 transistors coated with 0.24% and 1.2% OTS layers, we observed relatively high ΔV_{TH} values (1.42 V for 0.24% device and 1.92 V for 1.2% device) because many OTS molecules are affected by moisture in air. Although the p-doping effect is partially relieved during the first 60 h of air-exposure (18−34% loss of ΔV_{TH} initially achieved by OTS doping), it becomes stable in air after 60 h, and also the ΔV_{TH} loss is recovered again by an additional thermal anneal at 120 °C. In addition, we observed a very small reduction in the on-currents extracted at $V_{GS} - V_{TH}$ = −15 V after air exposure for 120 h. In the device doped by 1.2% OTS, the on-current was reduced by only ~31% (from ~68 μA to ~47 μA) after 36 h of air-exposure and by ~60% (from ~68 μA to ~27 μA) after 120 h. In the highly p-doped WSe_2 TFT by NO_2 reported by Peida *et al.*, the on-current decreased from ~22 to ~6 μA (~72% reduction) after 36 h of air exposure.[23] The on-current monitoring data for the other OTS-doped samples (0.024%, 0.12%, and 0.24%)

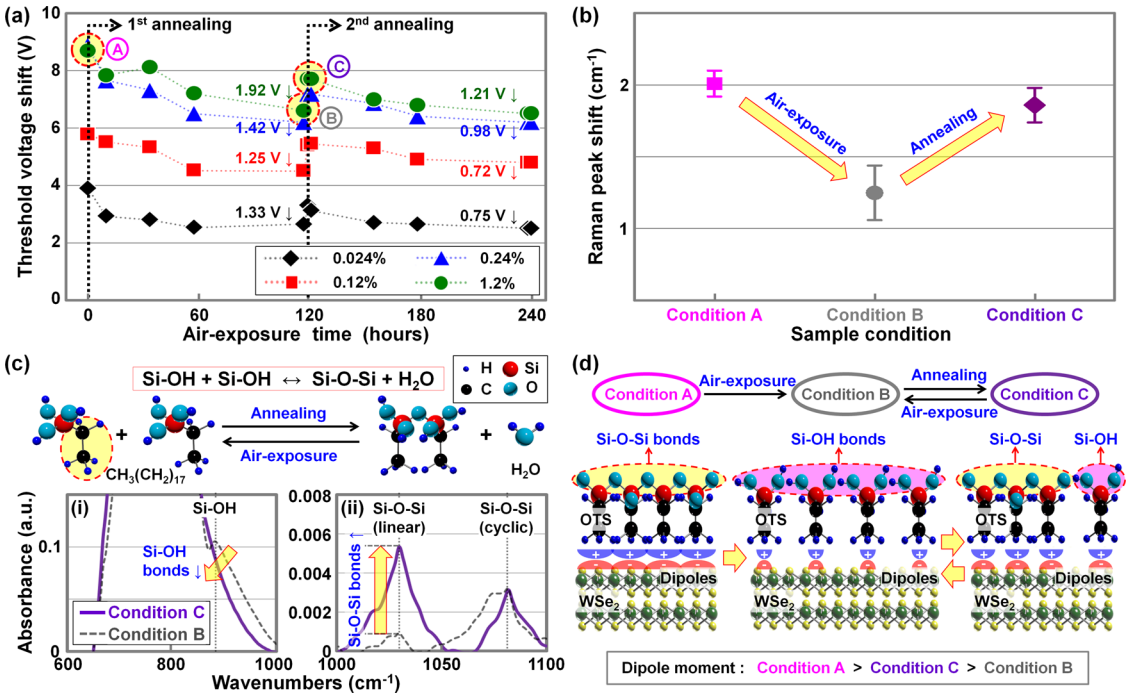

Figure 3. (a) Threshold voltage shift ($\Delta V_{TH} = V_{TH\text{-}OTS} - V_{TH\text{-}Control}$) of OTS-doped WSe_2 transistors as a function of air-exposure time. Here, after exposure to air for 120 h, the devices were annealed again at 120 °C. Condition A: right after OTS doping and annealing. Condition B: after air exposure for 120 h. Condition C: after additional 120 °C anneal. (b) Raman peak shift values of the three conditions, which were extracted from the peaks at 250 cm^{-1}. (c) Schematic diagram showing the possible chemical reaction between conditions B and C, and FT-IR spectra of OTS under conditions B and C ((i) Si−OH peak at ~880 cm^{-1} and (ii) Si−O−Si peak at ~1030 cm^{-1}). (d) Schematic diagrams predicting how chemical changes in OTS after long periods of air-exposure (condition B) and 120 °C recovery annealing (condition C) affect the dipole moments at the WSe_2−OTS interface.

can be found in Figure S4 (Supporting Information). Raman analysis performed on the WSe_2 samples under the three conditions also coincides with the V_{TH} and on-current monitoring data (condition A, right after OTS doping and annealing; condition B, after air exposure for 120 h; condition C, after air exposure for 120 h + additional 120 °C anneal). As shown in Figure 3b, Raman peak shift values extracted from the peaks at 250 cm^{-1} were reduced from 2.01 to 1.25 cm^{-1} after 120 h of air exposure, indicating a weakened p-doping phenomenon. However, the peak shift value was almost recovered (up to 1.86 cm^{-1} from 1.25 cm^{-1}) after an additional 120 °C anneal, as already confirmed in the previous V_{TH} and on-current monitoring experiment. Because the methyl (−CH_3) and polar head (−$SiCl_3$) functional groups in OTS have positive and negative poles, respectively, due to the asymmetric structure of OTS, the electron carrier density in WSe_2 in contact with the −CH_3 group is reduced, and consequently, the p-doping effect is apparent. The $SiCl_3$ almost immediately reacts with moisture and forms $Si(OH)_3$ when OTS is exposed in air. The −OH group attached to the Si atom is expected to react with another −OH group right after the 120 °C anneal. Consequently, it seems to form Si−O−Si bonds between OTS molecules (during this reaction, H_2O is also produced). After exposure of the devices to air for a long time, some of the Si−O−Si bonds are expected to break through reaction with H_2O, subsequently increasing Si−OH bonds. As shown in Figure 3c, we observed the FT-IR peak related with Si−OH bonds (~880 cm^{-1}) in the WSe_2 sample exposed to air for 120 h. However, this Si−OH bond disappeared after the 120 °C anneal and the peak for Si−O−Si bonds (~1030 cm^{-1}) increased, indicating that Si−O−Si bonds were formed again through the reaction between −OH groups. Therefore, as shown in Figure 3d, compared to the case of Si−O−Si bonding, the Si−OH formation in OTS seems to weaken the strength of positive charges (−CH_3 groups) and thereby the dipoles between OTS and WSe_2 (also, p-doping phenomenon). However, after a 120 °C anneal, it is thought that the additional Si−O−Si bonds formed through the reaction between −OH groups strengthen the dipoles and eventually the p-doping phenomenon on WSe_2. For reference, the V_{TH} value shifted only slightly (around −0.2 V) after annealing at 120 °C in the control device (undoped), which was much smaller than the shifts (0.65−1.1 V) in doped devices. However, an encapsulation layer that can effectively block moisture may ensure the air-stability of the p-doping phenomenon.

Characterization of OTS-Doped WSe_2 Optoelectronic Devices. To investigate the effect of the OTS-based controllable p-doping method on optoelectronic device performance, we performed a photocurrent measurement on the doped WSe_2 devices using a laser source with a

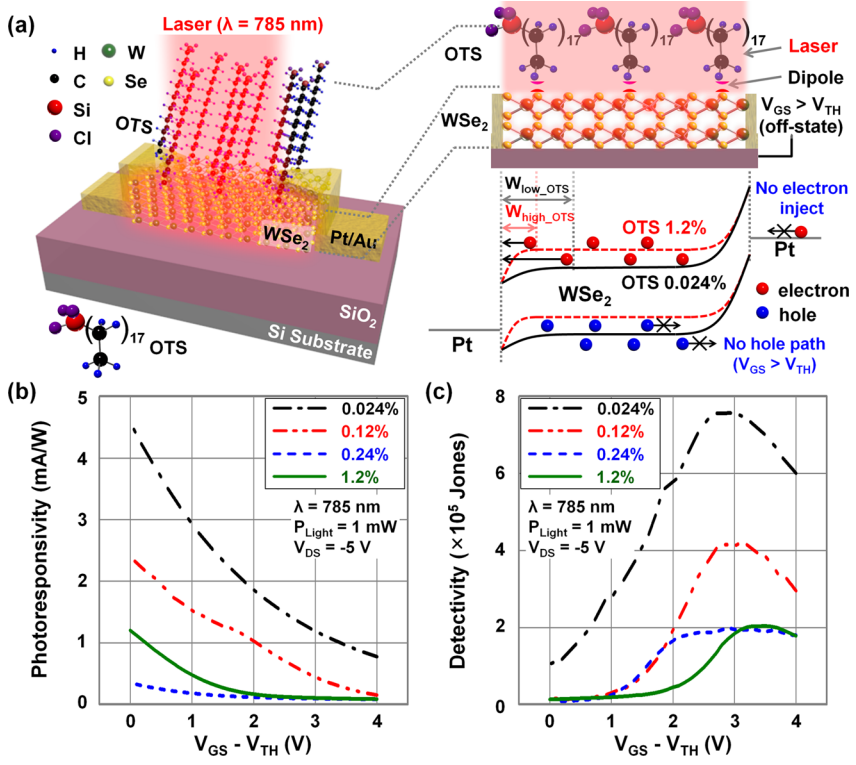

Figure 4. (a) Schematic diagrams showing the operation of an OTS-doped WSe_2 photodetector with a light source (λ = 785 nm and P = 1 mW) and the energy band diagrams of Pt−WSe_2−Pt junctions under the illuminated conditions. (b) Photoresponsivity and (c) detectivity as a function of $V_{GS} - V_{TH}$ (between 0 and 4 V in off-state) obtained on OTS-doped WSe_2 photodetectors (V_{DS} = −5 V).

wavelength of 785 nm. Figure 4a shows a schematic diagram of an OTS-doped WSe_2 photodetector device and the energy band diagram of Pt-undoped/doped WSe_2−Pt junctions with positive V_{GS} ($V_{GS} > V_{TH}$, off-state) and negative V_{DS} biases. As seen in the Supporting Information (Figure S3b), a photocurrent was not observed in the negative V_{GS} region (on-state) because of a high dark current level above 1.0×10^{-5} A/μm. In contrast, in the off-state (V_{GS} is positive and larger than V_{TH}), we clearly observed a photocurrent because the absence of hole paths in WSe_2 (low hole current) and the high electron barrier height (low electron current) reduced the dark current down to the order of 10^{-12} A/μm. When the level of p-doping was decreased by using a lower concentration OTS layer, a higher photocurrent was measured in the off-state. The increased depletion width seen on the left-side Pt−WSe_2 junction in Figure 4a might help collect more photogenerated electrons and eventually increase the photocurrent level in lightly doped WSe_2 devices ($W_{low\text{-}OTS} > W_{high\text{-}OTS} \rightarrow I_{Photo\text{-}low\text{-}OTS} > I_{Photo\text{-}high\text{-}OTS}$). The long diffusion length in lightly doped WSe_2 is also predicted to be another important reason for the increase in the photocurrent. We also note that the depletion width change in the right-side Pt−WSe_2 junction, which is relevant to hole carrier transport, can be neglected because the off-state WSe_2 region has no hole current path. Overall, the photocurrent increases as the p-doping level decreases because of broader depletion width and increased diffusion length. This rising trend in photocurrent (as the p-doping level decreases) can also be confirmed in the photoresponsivity and detectivity analyses shown in parts b and c, respectively, of Figure 4. Because photoresponsivity ($R = I_{Photo}/P_{Light}$) is proportional to photocurrent, the highest R value (~4.5 mA/W) is observed in the 0.024% OTS-doped WSe_2 device. Photoresponsivity values decrease in all doped WSe_2 devices as $V_{GS} - V_{TH}$ increases up to 4 V because it becomes harder to collect electron carriers in the left-side Pt−WSe_2 junction when a higher $V_{GS} - V_{TH}$ bias is applied. The highest detectivity (D^* = ~7.55×10^5 Jones) is observed in the WSe_2 device with the lowest doping concentration because the detectivity can be expressed as the ratio of I_{Photo} to I_{Dark}. Here, D^* is defined as $(RA^{1/2})/(2eI_{Dark})^{1/2}$, where R is photoresponsivity, A is the effective area of the device, e is the absolute value of the electron charge (1.6×10^{-19} C), and I_{Dark} is dark current. The decreased dark current at higher $V_{GS} - V_{TH}$ bias (Supporting Information, Figure S3) consequently increases the detectivity values in all of the doped WSe_2 devices. However, the detectivity starts decreasing beyond 3 V of $V_{GS} - V_{TH}$ because of an increase in dark current. The higher V_{GS} bias induces a higher electric field in the right-side Pt−WSe_2 junction, subsequently reducing the effective electron barrier height. In this photodetecting device experiment, we confirmed that it is possible to control the performance (photoresponsivity and detectivity) of

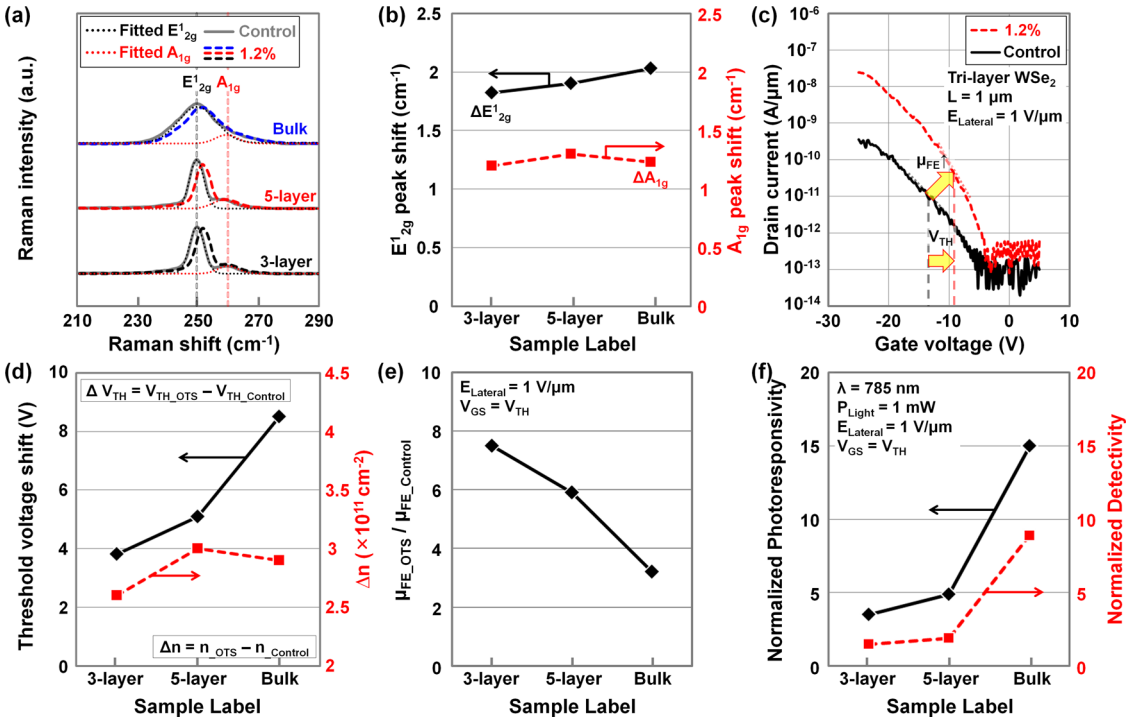

Figure 5. (a) Raman spectra of the 1.2% OTS-doped WSe_2 films and (b) extracted Raman peak shifts at E^1_{2g} and A_{1g} obtained in trilayer, few layer, and bulk WSe_2 samples. (c) I_D-V_G characteristics of the transistors fabricated on (black) undoped and (red) 1.2% OTS-doped trilayer WSe_2 films (L = 1 μm and $E_{Lateral}$ = 1 V/μm). Here, the I_D was normalized by channel width (W). (d) Threshold voltage shift ($\Delta V_{TH} = V_{TH\text{-}OTS} - V_{TH\text{-}Control}$) and carrier concentration increase ($\Delta n = n_{OTS} - n_{Control}$) of trilayer, few layer, and bulk WSe_2 device samples. (e) Field-effect mobility ratio ($\mu_{FE\text{-}OTS}/\mu_{FE\text{-}Control}$ at $V_{GS} = V_{TH}$) of trilayer, few layer, and bulk WSe_2 device samples. (f) Normalized photoresponsivity and detectivity of the 1.2% OTS-doped photodetectors fabricated on trilayer, few layer, and bulk WSe_2 films (λ = 785 nm, P_{Light} = 1 mW, $E_{Lateral}$ = 1 V/μm, and $V_{GS} = V_{TH}$).

an optoelectronic device (here, a photodetector) by adjusting the doping level of the TMD layer because the change in doping concentration affects the photocurrent *via* the depletion width (W) and the carrier diffusion length (L).

OTS Doping Characterization on WSe_2 Films of Various Thicknesses. To investigate the effect of WSe_2 thickness on OTS doping, we performed once again the Raman analysis and electrical/optical measurements on trilayer, few layer, and bulk WSe_2 device samples. As shown in Figure 5a, OTS doping was confirmed on the WSe_2 films of various thicknesses through Raman spectroscopy. Although a single peak was previously found at ~250 cm^{-1} on bulk WSe_2, one more peak was observed at 260 cm^{-1} on tri- and few layer WSe_2 films, which is thought to be the A_{1g} peak. For reference, Zeng *et al.* previously reported that two different WSe_2 Raman peaks appeared near 250 cm^{-1} (the E^1_{2g} peak) and 260 cm^{-1} (the A_{1g} peak).[25] After fitting the E^1_{2g} and A_{1g} Raman peaks (Supporting Information, Figure S6), we plotted ΔE^1_{2g} and ΔA_{1g} values extracted from the Raman peaks before/after 1.2% OTS doping, as shown in Figure 5b. Regardless of the number of WSe_2 layers, almost the same degree of peak shift was confirmed (1.8−2.0 cm^{-1} for ΔE^1_{2g} and 1.2−1.3 cm^{-1} for ΔA_{1g}), indicating that the OTS doping phenomenon is independent of the thickness of WSe_2. We then fabricated transistors on the three kinds of WSe_2 films and performed electrical/optical measurements. As shown in Figure 5c, even in the trilayer WSe_2 device, a positive shift in threshold voltage and an increase in field-effect mobility were observed after p-doping using a 1.2% OTS layer. The ΔV_{TH} values showed a decreasing tendency as the number of layers reduced (Figure 5d). It is thought that the lower intrinsic carrier concentration (n_i) of trilayer WSe_2 with larger energy bandgap makes the Fermi-level (E_F) farther away from the intrinsic energy level (E_i) than it is in the other WSe_2 samples. Subsequently, a stronger electric field that enables an increase in tunneling probability from metal to WSe_2 is expected on the metal-WSe_2 junction at the equilibrium state. Therefore, the additional electric field induced by OTS doping seems to exert less influence on the trilayer device sample, eventually producing the lowest ΔV_{TH} value (~3.81 V). However, in the case of 2D sheet doping concentration, similar values between 2.62 × 10^{11} and 3.0 × 10^{11} cm^{-2} in Δn (= $n_{OTS} - n_{Control}$) were observed. Those values agree with the Raman-analyzed results because the number of carriers supplied by OTS doping is independent of the thickness of the WSe_2 films. The field-effect mobility values of the doped devices normalized by those of control devices are between 3.2 and 7.5, as shown in Figure 5e, and it consequently indicates that mobility was enhanced through OTS doping in all WSe_2 devices. Compared to a WSe_2 top-surface exposed to air

(control device), top-surface passivation by an OTS coat seems to suppress top-surface scattering and thereby enhance mobility. In particular, this mobility improvement is expected to be more effective in thinner devices in which mobility degradation through top-surface scattering is more severe: the $\mu_{FE\text{-}OTS}/\mu_{FE\text{-}Control}$ value increases from 3.2 to 7.5 as the WSe_2 layer becomes thinner. Figure 5f shows the photoresponsivity and detectivity of the three kinds of WSe_2 devices (at $V_{GS} = V_{TH}$) normalized by the values of the control devices (before OTS doping). As already analyzed in the bulk WSe_2 device (Figure 4), enhancement in photoresponsivity and detectivity was also observed in the tri- and few layer devices, although those showed a decreasing tendency as the number of WSe_2 layers declined (normalized R from 15.2 to 3.5 and normalized D^* from 8.9 to 1.5). This enhancement occurs because a photocurrent increases with a broader depletion width and an increased diffusion length in the metal-WSe_2 junction region, which are achieved by OTS doping. However, in the thinner WSe_2 devices, the reduction in the amount of absorbed light seems to decrease the photoresponsivity and detectivity.

CONCLUSIONS

In conclusion, we demonstrated a controllable nondegenerate p-doping technique for 2D TMD materials (here, WSe_2) by adjusting the concentration of OTS in hexanes. This p-doping phenomenon is thought to originate from the fact that the methyl ($-CH_3$) functional groups in OTS have a positive pole and consequently reduce the electron carrier density in WSe_2. The controlled p-doping levels were between 2.1×10^{11} and 5.2×10^{11} cm^{-2} in the nondegenerate regime in which WSe_2-based electronic and optoelectronic devices can be properly designed. We also investigated the correlation between the controlled p-doping level and the performance parameters of WSe_2-based electronic and optoelectronic devices (V_{TH}↑, on-/off-currents↑, field-effect mobility↑, photoresponsivity↓, and detectivity↓ as the doping level increases). In addition, the p-doping effect by OTS was sustained in air for a long time with only small changes in the device performance (18−34% loss of ΔV_{TH} initially achieved by OTS doping for 60 h), and the degradation was almost completely recovered by additional thermal annealing at 120 °C. We also used Raman spectroscopy and electrical/optical measurements to confirm that OTS doping was independent of the thickness of the WSe_2 films. We expect our controllable p-doping method to make possible successful integration of future layered semiconductor devices.

EXPERIMENTAL METHODS

Formation and Doping Control of OTS on WSe_2 Film. Various thicknesses of WSe_2 nanoflakes (trilayer, few layer, and bulk) were transferred onto a 90 nm thick dry-oxidized SiO_2 layer grown on a heavily doped p-type Si substrate (resistivity <0.005 Ω-m) by adhesive tape, and the samples were washed with acetone for 1 h to remove the tape residue. The number of layers for trilayer, few layer, and bulk WSe_2 flakes was identified by AFM (Supporting Information, Figure S5). For the formation of the OTS layer on WSe_2 samples, different amounts of OTS (12, 60, 120, and 600 μL) were added to 50 mL of hexane (a mixture of isomers), and the WSe_2 samples were soaked in each solution for 1 h. After that, the samples were rinsed with toluene, acetone, and deionized water several times and baked at 120 °C for 20 min.

Characterization of OTS-Doped WSe_2 Films. OTS/WSe_2/SiO_2/Si samples were investigated and compared with a control sample (WSe_2/SiO2/Si) by FT-IR (Bruker IFS-66/S) and PL/Raman spectroscopy (Alpha300 M+, WITec) measurements. The FT-IR spectral range was between 4000 and 20 cm^{-1}, the scan rate was 110 scans/s, and the resolution was above 0.1 cm^{-1}. A Raman spectroscope with an excitation wavelength of 532 nm was used, the laser beam size was 0.7−0.9 μm, and the instrumental spectral resolution was below 0.9 cm^{-1}. An integration time of 5 s and a spectrometer with 1800 grooves/mm were used for the test.

Fabrication and Electrical Characterization of an OTS-Doped WSe_2 Electronic Device. For the fabrication of back-gated WSe_2 transistors, we patterned source/drain electrodes (channel length and width of 5 μm) on WSe_2/SiO_2/Si samples by optical lithography, followed by Pt (10 nm) and Au (50 nm) deposition in an e-beam evaporator. To fabricate the transistor devices on thin (trilayer or few layer) WSe_2 films, e-beam lithography instead of optical lithography. Transistors were doped (or coated) by different concentrations of OTS (0.024%, 0.12%, 0.24%, and 1.2%) and were electrically analyzed using an HP 4415B semiconductor parameter analyzer (I_D-V_G and I_D-V_D) and an HP 4284A precision LCR meter (C-V). The threshold voltage (V_{TH}), carrier concentration (n), and field-effect mobility (μ_{FE}) were calculated from the I_D-V_G data. Parameter extraction is explained in the Supporting Information (Figure S1). We used the equations $n = I_D L/qW\mu V_{DS}$ and $\mu_{FE} = L/(WV_{DS}C_{OX}) \times (\partial I_D/\partial V_{GS})$ at $V_{GS} = V_{TH}$, where q is the electron charge, L and W are the length and width of the channel, respectively, and C_{OX} is $\varepsilon_{OX} \times \varepsilon_0/t_{OX}$, which is the gate oxide capacitance per unit area.

Characterization of an OTS-Doped WSe_2 Optoelectronic Device. To investigate the optoelectronic properties of the fabricated OTS-doped WSe_2 devices, a current−voltage (I_D-V_G) measurement was performed under dark and illuminated conditions. The light sources were set up using a dot laser with a wavelength of 785 nm and an optical power of 1 mW. For the characterization and comparison of the WSe_2 optoelectronic devices doped with OTS at different concentrations (0.024%, 0.12%, 0.24%, and 1.2%), photoresponsivity (R) and detectivity (D^*) were calculated from the I_D-V_G curves: $R = I_{Photo}/P_{Light}$ and $D^* = (RA^{1/2})/(2eI_{Dark})^{1/2}$ at the off-state ($V_{GS} > V_{TH}$), where I_{Photo} is the generated photocurrent, P_{Light} is the total incident optical power, A is the effective area of detector, e is the absolute value of the electron charge (1.6×10^{-19} C), and I_{Dark} is the dark current.

Conflict of Interest: The authors declare no competing financial interest.

Acknowledgment. This work was supported by the Basic Science Research Program and Midcareer Researcher Program through the National Research Foundation of Korea (NRF) funded by the Ministry of Education, Science and Technology (Grant Nos. 2011-0007997 and 2012R1A2A2A02046890) and a Human Resources Development program grant (No. 20144030200580) of the Korea Institute of Energy Technology Evaluation and Planning (KETEP) funded by the Korean government Ministry of Trade, Industry and Energy.

Supporting Information Available: Extraction of electrical parameters (V_{TH}, μ_{FE}, n, and on-current). $C-V$ characterization of undoped and OTS-doped WSe_2 TFTs. Extraction of photoresponsivity (R) and detectivity (D^*). On-current monitoring of the OTS-doped WSe_2 TFTs. AFM analysis of the WSe_2 flakes used in this experiment. Fitting lines for the E^1_{2g} and A_{1g} peaks of control and OTS 1.2%-doped WSe_2 samples. This material is available free of charge *via* the Internet at http://pubs.acs.org.

REFERENCES AND NOTES

1. Radisavljevic, B.; Radenovic, A.; Brivio, J.; Giacometti, V.; Kis, A. Single-Layer MoS_2 Transistors. *Nat. Nanotechnol.* **2011**, *6*, 147–150.
2. Liu, W.; Kang, J.; Sarkar, D.; Khatami, Y.; Jena, D.; Banerjee, K. Role of Metal Contacts in Designing High-Performance Monolayer n-Type WSe_2 Field Effect Transistors. *Nano Lett.* **2013**, *13*, 1983–1990.
3. Bertolazzi, S.; Brivio, J.; Kis, A. Stretching and Breaking of Ultrathin MoS_2. *ACS Nano* **2011**, *5*, 9703–9709.
4. Pu, J.; Li, L. J.; Takenobu, T. Flexible and Stretchable Thin-Film Transistors based on Molybdenum Disulphide. *Phys. Chem. Chem. Phys.* **2014**, *16*, 14996–15006.
5. Mak, K. F.; Lee, C.; Hone, J.; Shan, J.; Heinz, T. F. Atomically Thin MoS_2: A New Direct-Gap Semiconductor. *Phys. Rev. Lett.* **2010**, *105*, 136805.
6. Chuang, S.; Kapadia, R.; Fang, H.; Chia Chang, T.; Yen, W.-C.; Chueh, Y.-L.; Javey, A. Near-Ideal Electrical Properties of InAs/WSe_2 Van Der Waals Heterojunction Diodes. *Appl. Phys. Lett.* **2013**, *102*, 242101.
7. Tonndorf, P.; Schmidt, R.; Bottger, P.; Zhang, X.; Borner, J.; Liebig, A.; Albrecht, M.; Kloc, C.; Gordan, O.; Zahn, D. R. T. et al. Photoluminescence Emission and Raman Response of Monolayer MoS_2, $MoSe_2$, and WSe_2. *Opt. Express* **2013**, *21*, 4908–4916.
8. Yin, Z.; Li, H.; Li, H.; Jiang, L.; Shi, Y.; Sun, Y.; Lu, G.; Zhang, Q.; Chen, X.; Zhang, H. Single-Layer MoS_2 Phototransistors. *ACS Nano* **2012**, *6*, 74–80.
9. Lee, H. S.; Min, S. W.; Chang, Y. G.; Park, M. K.; Nam, T.; Kim, H.; Kim, J. H.; Ryu, S.; Im, S. MoS_2 Nanosheet Phototransistors with Thickness-Modulated Optical Energy Gap. *Nano Lett.* **2012**, *12*, 3695–3700.
10. Zeng, H.; Dai, J.; Yao, W.; Xiao, D.; Cui, X. Valley Polarization in MoS_2 Monolayers by Optical Pumping. *Nat. Nanotechnol.* **2012**, *7*, 490–493.
11. Mak, K. F.; He, K.; Shan, J.; Heinz, T. F. Control of Valley Polarization in Monolayer MoS2 by Optical Helicity. *Nat. Nanotechnol.* **2012**, *7*, 494–498.
12. Lopez-Sanchez, O.; Lembke, D.; Kayci, M.; Radenovic, A.; Kis, A. Ultrasensitive Photodetectors Based on Monolayer MoS_2. *Nat. Nanotechnol.* **2013**, *8*, 497–501.
13. Kim, S.; Konar, A.; Hwang, W. S.; Lee, J. H.; Lee, J.; Yang, J.; Jung, C.; Kim, H.; Yoo, J. B.; Choi, J. Y.; et al. High-Mobility and Low-Power Thin-Film Transistors based on Multilayer MoS_2 Crystals. *Nat. Commun.* **2012**, *3*, 1011.
14. Fang, H.; Chuang, S.; Chang, T. C.; Takei, K.; Takahashi, T.; Javey, A. High-Performance Single Layered WSe_2 p-FETs with Chemically Doped Contacts. *Nano Lett.* **2012**, *12*, 3788–3792.
15. Fang, H.; Tosun, M.; Seol, G.; Chang, T. C.; Takei, K.; Guo, J.; Javey, A. Degenerate n-Doping of Few-Layer Transition Metal Dichalcogenides by potassium. *Nano Lett.* **2013**, *13*, 1991–1995.
16. Chen, M.; Nam, H.; Wi, S.; Ji, L.; Ren, X.; Bian, L.; Lu, S.; Liang, X. Stable Few-Layer MoS_2 Rectifying Diodes Formed by Plasma-Assisted Doping. *Appl. Phys. Lett.* **2013**, *103*, 142110.
17. Sreeprasad, T. S.; Nguyen, P.; Kim, N.; Berry, V. Controlled, Defect-Guided, Metal-Nanoparticle Incorporation Onto MoS_2 *via* Chemical and Microwave Routes: Electrical, Thermal, and Structural Properties. *Nano Lett.* **2013**, *13*, 4434–4441.
18. Du, Y. C.; Liu, H.; Neal, A. T.; Si, M. W.; Ye, P. D. Molecular Doping of Multilayer MoS_2 Field-Effect Transistors: Reduction in Sheet and Contact Resistances. *IEEE Electron Device Lett.* **2013**, *34*, 1328–1330.
19. Li, Y.; Xu, C. Y.; Hu, P.; Zhen, L. Carrier Control of MoS_2 Nanoflakes by Functional Self-Assembled Monolayers. *ACS Nano* **2013**, *7*, 7795–7804.
20. Najmaei, S.; Zou, X.; Er, D.; Li, J.; Jin, Z.; Gao, W.; Zhang, Q.; Park, S.; Ge, L.; Lei, S.; et al. Tailoring The Physical Properties of Molybdenum Disulfide Monolayers by Control of Interfacial Chemistry. *Nano Lett.* **2014**, *14*, 1354–1361.
21. Yun, D.-J.; Rhee, S.-W. Self-Assembled Monolayer Formation on Molybdenum with Octadecyltrichlorosilane and Phenethyltrichlorosilane and Measurement of Molybdenum−Pentacene Interface Properties. *J. Electrochem. Soc.* **2008**, *155*, H357.
22. Chakraborty, B.; Bera, A.; Muthu, D. V. S.; Bhowmick, S.; Waghmare, U. V.; Sood, A. K. Symmetry-Dependent Phonon Renormalization in Monolayer MoS_2 Transistor. *Phys. Rev. B* **2012**, *85*, 161403.
23. Zhao, P.; Kiriya, D.; Azcatl, A.; Zhang, C.; Tosun, M.; Liu, Y.-S.; Hettick, M.; Kang, J. S.; Mcdonnell, S.; Santosh, K. C.; et al. Air Stable p-Doping of WSe_2 by Covalent Functionalization. *ACS Nano* **2014**, *8*, 10808–10814.
24. Chen, C.-H.; Wu, C.-L.; Pu, J.; Chiu, M.-H.; Kumar, P.; Takenobu, T.; Li, L.-J. Hole Mobility Enhancement and p-Doping in Monolayer WSe_2 by Gold Decoration. *2D Mater.* **2014**, *1*, 034001.
25. Zeng, H.; Liu, G.-B.; Dai, J.; Yan, Y.; Zhu, B.; He, R.; Xie, L.; Xu, S.; Chen, X.; Yao, W.; et al. Optical Signature of Symmetry Variations and Spin-Valley Coupling in Atomically Thin Tungsten Dichalcogenides. *Sci. Rep.* **2013**, *3*, 1608.